Journal of proteome research

Article

pubs.acs.org/jpr

Mass Spectrometry and Antibody-Based Characterization of Blood Vessels from *Brachylophosaurus canadensis*

Timothy P. Cleland,[*,†,■] Elena R. Schroeter,[‡] Leonid Zamdborg,[§] Wenxia Zheng,[‡] Ji Eun Lee,[§,∥] John C. Tran,[⊥] Marshall Bern,[#] Michael B. Duncan,[▽,○] Valerie S. Lebleu,[▽,○,◆] Dorothy R. Ahlf,[⊥] Paul M. Thomas,[⊥] Raghu Kalluri,[▽,○,◆,¶] Neil L. Kelleher,[⊥] and Mary H. Schweitzer[‡,□]

[†]Marine, Earth and Atmospheric Sciences, [‡]Department of Biological Sciences, North Carolina State University, Raleigh, North Carolina 27695, United States

[§]Department of Chemistry, University of Illinois, Urbana, Illinois 61801, United States

[∥]Center for Theragnosis, Biomedical Research Institute, Korea Institute of Science and Technology, Hwarang-ro 14-gil 5, Seongbuk-gu, Seoul 136-791, Republic of Korea

[⊥]Departments of Chemistry, Molecular Biosciences and the Proteomics Center of Excellence, Northwestern University, Evanston, Illinois 60208, United States

[#]Protein Metrics, San Carlos, California 94070, United States

[▽]Division of Matrix Biology, Beth Israel Deaconess Medical Center, Boston, Massachusetts 02115, United States

[○]Department of Medicine, Harvard Medical School, Boston, Massachusetts 02115, United States

[◆]Department of Cancer Biology, Metastasis Research Center, University of Texas MD Anderson Cancer Center, Houston, Texas 77054, United States

[¶]Department of Biological Chemistry and Molecular Pharmacology and Harvard-MIT Division of Health Sciences and Technology, Harvard University, Cambridge, Massachusetts 02139, United States

[□]North Carolina Museum of Natural Sciences, Raleigh, North Carolina 27601, United States

Supporting Information

ABSTRACT: Structures similar to blood vessels in location, morphology, flexibility, and transparency have been recovered after demineralization of multiple dinosaur cortical bone fragments from multiple specimens, some of which are as old as 80 Ma. These structures were hypothesized to be either endogenous to the bone (i.e., of vascular origin) or the result of biofilm colonizing the empty osteonal network after degradation of original organic components. Here, we test the hypothesis that these structures are endogenous and thus retain proteins in common with extant archosaur blood vessels that can be detected with high-resolution mass spectrometry and confirmed by immunofluorescence. Two lines of evidence support this hypothesis. First, peptide sequencing of *Brachylophosaurus canadensis* blood vessel extracts is consistent with peptides comprising extant archosaurian blood vessels and is not consistent with a bacterial, cellular slime mold, or fungal origin. Second, proteins identified by mass spectrometry can be localized to the tissues using antibodies specific to these proteins, validating their identity. Data are available via ProteomeXchange with identifier PXD001738.

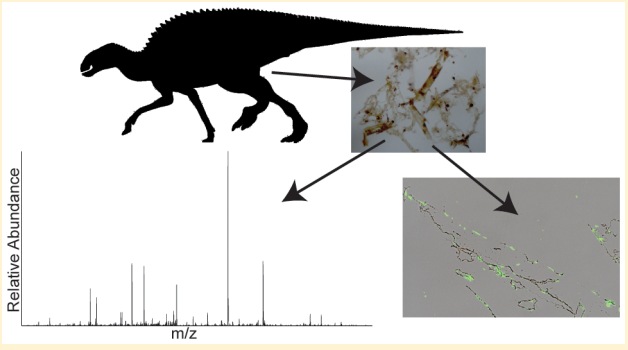

KEYWORDS: *Brachylophosaurus canadensis, blood vessels, dinosaur, cytoskeleton, actin, tubulin, myosin, tropomyosin, taphonomy, preservation*

INTRODUCTION

The paleoproteomic analysis of collagen I peptides from *Tyrannosaurus rex* (MOR 1125)[1] was controversial when first reported. The survival of proteins from the Cretaceous Period (66−145 million years ago) was not thought to be possible, and the statistical significance of the peptide identifications was questioned.[2,3] Higher-resolution detection of collagen I peptides from a *Brachylophosaurus canadensis* (MOR 2598)[4] were less controversial, but the detection and sequencing of ancient proteins from taxa other than these two dinosaurs still remain limited to 1.5 Ma or younger bone.[2,5−21]

Received: July 19, 2015
Published: November 23, 2015

DOI: 10.1021/acs.jproteome.5b00675
J. Proteome Res. 2015, 14, 5252−5262

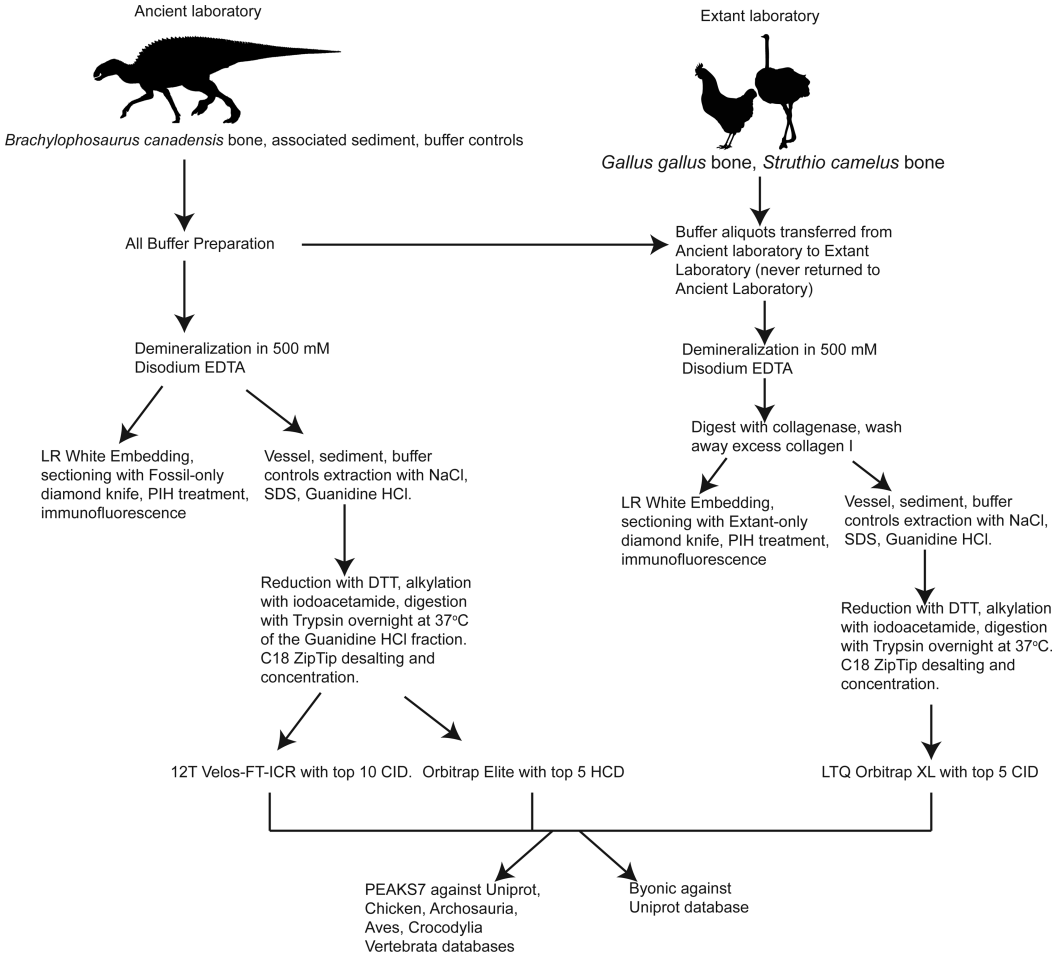

Figure 1. Flowchart of experimental procedures, laboratories, and specimens used in this study.

Although soft tissue vessels and cells have been observed in multiple fossil specimens in addition to these two dinosaurs,[22−24] continued skepticism on the prevalence and endogeneity of ancient soft tissues and their composite molecules persists. However, a recent report of collagen fibrils (based on TEM banding patterns) and erythrocyte-like structures[25] renewed interest in the possibility that original structures and their molecular constituents can be chemically characterized in Cretaceous fossils.

Chemical methods capable of differentiating between endogenous and microbial origins must be employed to ascertain the source of the soft tissues, especially those that can provide peptide sequence information. If these structures are derived from bacterial biofilm or fungi growing within the empty osteonal network,[26] then they should not yield vertebrate peptides, only bacterial or fungal proteins. Alternatively, if these biomaterials are endogenous to the dinosaurs, then they should retain recognizable fragments of proteins consistent with vertebrate blood vessels or the cells or proteins (e.g., actin, tubulin[27]) that comprise them in extant vertebrate taxa. It should be recognized, however, that at any point in diagenesis environmental microbes associated with burial sediments could coexist with vertebrate proteins from endogenous sources. Thus, identification of microbial proteins together with vertebrate proteins would not preclude their authenticity.

We have chosen to focus on protein recovery and identification in these Cretaceous fossils instead of DNA because (1) protein longevity is hypothesized to be greater than that of DNA,[28] so proteins have an increased chance of persisting into deep time. (2) The detection and confirmation of proteinaceous material in fossils can be validated using a plethora of methods, including antibody localization, mass spectrometry sequencing, gel electrophoresis, enzyme specificity through digestion, specific stains, and identification of amide bonds using high-resolution spectroscopic methods (e.g., synchrotron analyses).[29] These allow for independent confirmation of their presence and are not applicable to DNA. (3) Detection of in vivo post-translational modifications (PTMs) may elucidate protein function that cannot be extrapolated from DNA sequences alone; detection of diagenetic PTMs may allow formulation of hypotheses to explain preservation or protein degradation processes.

To optimize the recovery of endogenous proteins that are of lower abundance, but which may be more informative than collagen in living tissues, we isolated vessels by first demineralizing cortical bone from the tibia of a *B. canadensis* (MOR 2598[4]) specimen for extraction rather than using whole bone extracts, which, in extant vertebrates, are dominated by collagen. Because birds are the closest living relatives of dinosaurs, blood vessels were also isolated from extant, demineralized ostrich and chicken bones by demineralization, then the collagen I matrix was removed through specific collagenase digestion. Ostrich vessels were used as a positive control in immunohistochemical analyses, and ostrich and chicken vessels were used as positive controls for mass

DOI: 10.1021/acs.jproteome.5b00675
J. Proteome Res. 2015, 14, 5252−5262

spectrometry studies. All ancient tissues were processed in a designated laboratory completely separated from the extant controls to prevent contamination (see Materials and Methods; Figure 1).

MATERIALS AND METHODS

For clarity of this section, we have included a flowchart of procedures described below (Figure 1).

Blood Vessel Collection

In a laboratory dedicated to analyses of fossil tissues, exclusive of any extant material, cortical bone fragments (~2 g) from the *B. canadensis* femur (MOR 2598; provenance and storage conditions described previously[4]) were demineralized in 500 mM sterilized ethylenediaminetetraacetic acid (EDTA) (pH 8.0) in a glass Kimax crystallizing dish to prevent the addition of plasticizers detectable by mass spectrometry. EDTA was exchanged once or twice daily until complete demineralization was accomplished (i.e., only soft tissue residue remained). Vessels were collected inside a sterile laminar flow hood with a cut-tip pipet to prevent contamination and washed with e-pure water to remove residual EDTA. After washing, the vessels were stored in water at 4 °C until extraction or embedding.

In a separate laboratory designated for analyses of extant material, cortical bone fragments from ostrich femur were demineralized in 500 mM EDTA (pH 8.0) until all mineral was removed, leaving a flexible and fibrous collagenous matrix, with little resistance to cutting with a razor blade. After demineralization, ~1 mm thick slices were cut, washed 10–20 times with e-pure water to remove EDTA, and then digested overnight at 37 °C in 2 mL of 1 mg/mL collagenase A (Roche) diluted in Dulbecco's phosphate buffered saline to liberate vessels, cells, and other noncollagenous components. The liberated vessels were washed to remove residual collagenase and stored at 4 °C until extraction or fixation. Half of the ostrich blood vessels were subjected to extraction (below), and half were fixed overnight at room temperature in neutral buffered 10% formalin.

Blood Vessel Protein Extraction

B. canadensis (7.5–8 mg), chicken (~10 mg), and ostrich (~11 mg) blood vessels were chemically extracted following the protocol in Didangelos et al.[30] As with initial vessel collection, fossil and extant tissues were processed in separate, designated laboratories using separate buffers and equipment. *B. canadensis* vessels, environmental control of 7.6 mg sediments from the dinosaur burial environment, and a buffer control (i.e., all buffers treated in tandem with bone and sediment but with no sample added) were incubated in 900 μL screw cap spin columns (Pierce) and centrifuged at 3263 rpm for 1 min between each step; ostrich vessels were incubated in 1.5 mL centrifuge tubes and centrifuged 2000 rpm for 2 min to separate the pellet from the supernatant. All blood vessels were incubated in 200 μL of 0.5 M NaCl, 10 mM Tris (pH 7.3) for 4 h with gentle vortexing, supernatant was collected, and then the pellet was incubated for 4 h in 200 μL of 0.08% SDS and vortexed as above. The SDS supernatant was collected, and the remaining pellet was incubated for 48 h in 200 μL of 4 M guanidine HCl in 50 mM sodium acetate (pH 5.8). The supernatant was collected, and then all supernatants (NaCl, SDS, and guanidine HCl) were centrifuged at 13 200 rpm for 10 min to pellet any remaining debris. Debris-free supernatants were transferred to weighed tubes using sterile pipettes. Proteins suspended in the supernatant were precipitated from the NaCl and SDS using 800 μL of acetone overnight at −20 °C. Proteins were precipitated from the guanidine HCl supernatant using 1 mL of 100% ethanol overnight at −20 °C. Precipitated proteins were pelleted at 13 200 rpm for 10 min, and supernatant was removed by tube inversion. The protein pellet from the guanidine HCl extraction was washed once more with 250 μL of 95% ethanol to remove any residual guanidine HCl, centrifuged, and inverted to remove any remaining ethanol. All tubes were allowed to air-dry inside a sterile laminar flow hood, weighed, and stored at −80 °C until used for mass spectrometry.

Tryptic Digestion

Protein pellets from extracts of *B. canadensis*, sediment, buffer control, chicken, and ostrich were resuspended in 30–50 μL of 50 mM ammonium bicarbonate, reduced for 1 h at 37 °C with 10 mM dithiothreitol (i.e., 0.5 μL of 1 M dithiothreitol/50 μL of ammonium bicarbonate), and then alkylated for 1 h in the dark with 20 mM iodoacetamide (i.e., 1 μL of 1 M iodoacetamide/50 μL of ammonium bicarbonate). Proteins were digested with 0.12 μg of Promega modified trypsin overnight (~18 h) at 37 °C. We used this reduced concentration of enzyme because we expected *B. canadensis* protein to be very low in concentration and we did not want to overwhelm the endogenous signal with exogenous trypsin. After digestion, all samples were acidified with 1 μL of 100% formic acid. Peptides were concentrated by eluting from ZipTips (Millipore) with 50% acetonitrile, 0.1% formic acid into 10 μL aliquots.

Reverse-Phase Nanocapillary Liquid Chromatography

All peptides were eluted with the following gradient: 2% B at start, 60% B at 30 min, 90% B at 32 min, 90% B at 35 min, 2% B at 37 min, 2% B at 60 min. Buffer A was 95% water, 5% ACN, 0.1% formic acid, and Buffer B was 95% acetonitrile, 5% water, 0.2% formic acid.

Ostrich and chicken peptides were injected onto a Waters nanoAcquity UPLC trap column (180 μm × 20 mm) with Symmetry C18 and washed for 5 min at 5 μL/min. Peptides were transferred to a Waters nanoAcquity UPLC (75 μm × 250 mm) BEH130C18 (1.7 μm particle size) analytical column and eluted at 300 nL/min on a Waters nanoAcquity.

B. canadensis peptides in 0.1% formic acid were injected onto a self-packed trap column (150 μm i.d., 2 cm bed length, C18 125 Å pore size, 3 μm particle size (Phenomenex)) and washed for 10 min at 3 μL/min. Peptides were transferred to and eluted from a self-packed analytical column (75 μm i.d., 10 cm bed length, C18 125 Å pore size, 3 μm particle size (Phenomenex)) with a picofrit emitter tip at 300 nL/min with a Dionex nano-HPLC system (Thermo Fisher Scientific).

Mass Spectrometry Data Acquisition

Ostrich and chicken peptides were detected on an LTQ Orbitrap XL (Thermo Fisher Scientific) with a scan range of 375–2000 m/z. The top five most intense peaks for each precursor scan were fragmented using collision-induced dissociation (CID) with an isolation window of 2 m/z. Dynamic exclusion was enabled with a repeat count of 1, exclusion duration of 10 s, and a repeat duration of 30 s.

B. canadensis peptides were detected with a 12T Velos FT-ICR (Thermo Fisher Scientific) or a Velos Orbitrap Elite (Thermo Fisher Scientific) with a scan range of 350–2000 m/z. Neither of these instruments had avian proteins run on them to prevent any question of intra-instrument contamination, even

DOI: 10.1021/acs.jproteome.5b00675
J. Proteome Res. 2015, 14, 5252–5262

after the dinosaur peptides had been analyzed. For the 12T Velos FT-ICR, the top 10 most intense peaks for each precursor scan were fragmented using CID with an isolation window of 2 m/z. Dynamic exclusion was enabled with a repeat count of 1, exclusion duration of 240 s, and a repeat duration of 5000 s. Exclusion mass width was set to ± 1.50 m/z. On the Velos Orbitrap Elite, the top five most intense peaks for each precursor scan were fragmented using higher energy collisional dissociation (HCD) with an isolation width of 2 m/z. The minimum FT mass for fragments was set at 125 m/z. On all instruments, unassigned and 1+ charged molecules were rejected for fragmentation. All buffer and sediment controls were injected before the *B. canadensis* extractions to account for potential contamination within the nanoLC systems.

Database Analysis

All *B. canadensis* spectra were searched in Byonic 1.1 (Protein Metrics, San Carlos, CA) using a 10 ppm mass accuracy for precursors and either 0.4 Da (for ion-trap MS2) or 20 ppm (for Orbitrap MS) for fragment ions. We allowed for up to two missed cleavages and set carbamidomethylated cysteine as fixed. Deamidated asparagine and glutamine; pyro-glu N-terminal glutamine, glutamic acid, and carbamidomethylated cysteine; oxidized methionine and tryptophan; and doubly oxidized tryptophan were set as variable. An initial search used the full SwissProt database, and a subsequent wildcard search, which allowed one unknown modification per peptide of any mass between −120 and +120 Da, was conducted on proteins identified in the initial search. A wildcard search finds unanticipated modifications and sequence variants, but it is less sensitive to exact matches due to the increased size of the search space. FDR was calculated using target-decoy reverse-database searching and restricted to 1%.

All spectra were also searched in PEAKS7[31,32] using the same parameters as those used for Byonic. Additionally, PEAKS7 searches were performed with a 10 ppm mass accuracy for precursors and 0.5 Da for fragment ions of CID spectra and 5 ppm/0.02 Da for HCD spectra. Up to five miss cleavages were allowed, as was nonspecific cleavage at either end of the peptides. No fixed modifications were specified. Oxidation of methionine and deamidation of asparagine and glutamine were allowed as variable modifications. All *B. canadensis* spectra were searched against the following separate databases: UniProt Vertebrates, UniProt Chicken, NCBI Archosauria (Aves + Crocodylia), NCBI Crocodylia, and NCBI Aves. All chicken and ostrich spectra were searched against UniProt Chicken, and ostrich GuHCl spectra were additionally searched against UniProt Vertebrates. To find additional, unspecified PTMs and mutations, PEAKS PTM and SPIDER were enabled. Results were filtered with the following parameters: peptide spectral match FDR $\leq 5\%$, proteins ≥ -10 IgP 20 plus at least 1 unique peptide. These relaxed parameters allow for potential detection of nontryptic peptides. Common laboratory contamination is included in all UniProt searches.

Fragmentation spectra were exported from Qualbrowser to allow for deamidation analysis using Isotopica.[33] Partial sequences of the N-terminus (−0.1 Da offset) or C-terminus (+18.0105 Da offset) were used to quantify singly, doubly, or triply deamidated peptides. All values are reported as %QN or the amount of glutamine and/or asparagine remaining.

Spectra and result files are available at the ProteomeXchange Consortium (http://proteomecentral.proteomexchange.org) via the PRIDE partner repository[34] with the data set identifier PXD001738.

Peptide Alignment and Phylogenetic Analysis

All candidate peptides from *B. canadensis* were aligned to their respective protein from a large number of bird and alligator species (Table S1) using Seaview 4.4.2[35] or ClustalX 2.1.[36] Consensus sequences for all proteins were generated in Seaview 4.4.2. After alignment, Tree analysis using New Technology (TNT[37]) files were generated using Mesquite 2.75.[38] In TNT, the myosin sequences were searched using traditional searches with 1000 random seeds, 10 000 replicates, and 10 stored trees per replicate. Bremer support and Jackknife (10 000 resamples) were used to support the branches.

Immunofluorescence

Because iron has been previously observed in these and other fossil vessels,[4,15,22,39] *B. canadensis* vessels were incubated overnight in 5 mM pyridoxal isonicotinic hydrazide (PIH) in 50 mM NaOH to remove iron from vessel walls.[40,41] PIH-treated *B. canadensis* and 10% formalin fixed ostrich blood vessels were embedded in LR White resin blocks after partial dehydration in 70% ethanol. Six to eight 200 nm sections were taken on a Leica EM UC6 ultramicrotome and dried overnight at 45 °C to each well of a 6-well Teflon-coated slide (Electron Microscopy Sciences). Antigen retrieval and quenching of autofluorescence were performed with two incubations in 500 mM EDTA, pH 8.0, and two incubations in 1 mg/mL sodium borohydride for 10 min each. Spurious binding was inhibited by incubating sections in 4% normal goat serum (NGS) for 2 h at room temperature. Treated sections were incubated overnight at 4 °C in either primary antibody (Table S2) diluted to final concentration in 4% NGS or only 4% NGS (no primary) to control for nonspecific binding of secondary antibody. Antiserum to human testosterone, a short-lived mammalian hormone not expected to be present in archosaur tissues, was used at the same concentration as test antibodies to function as an irrelevant, negative control for nonspecific binding of primary antibody. No response was expected. To test the specificity of each primary antibody, they were incubated with excess immunogen at RT for 4 h and then at 4 °C for 1 week with their specific protein (Table S3). This served to fully occupy binding sites in the antibody, making them unavailable to bind epitopes in tissue. The inhibited antibodies were applied to sections, using the same parameters as above. Binding observed in the test conditions should be reduced or absent in sections exposed to inhibited antibodies.

After incubation with primary antibodies or controls overnight at 4 °C, sections were washed once with phosphate buffered saline (PBS) modified with 0.05% Tween-20 and then twice with PBS (no Tween-20) to remove excess primary antibody. All sections were then incubated for 2 h in secondary antibody (biotinylated goat anti-rabbit IgG diluted (1:500) in PBS) and then for 1 h in avidin fluorescein isothiocyanate (FITC) (1:1000), each separated by multiple washes in PBS/Tween-20 and PBS as described above.

Sections were imaged on a Zeiss AxioSkop 2 plus with an AxioCam MRc 5 and integrated using AxioVision software (version 4.7.0.0). Ostrich immunofluorescence images were acquired for 100 ms. Brightness was set to −0.34, contrast was set to 2.19, and gamma was set to 0.29 and held constant across all samples. *B. canadensis* immunofluorescence images were also acquired for 100 ms. Brightness was set to −0.34, contrast was

DOI: 10.1021/acs.jproteome.5b00675
J. Proteome Res. 2015, 14, 5252−5262

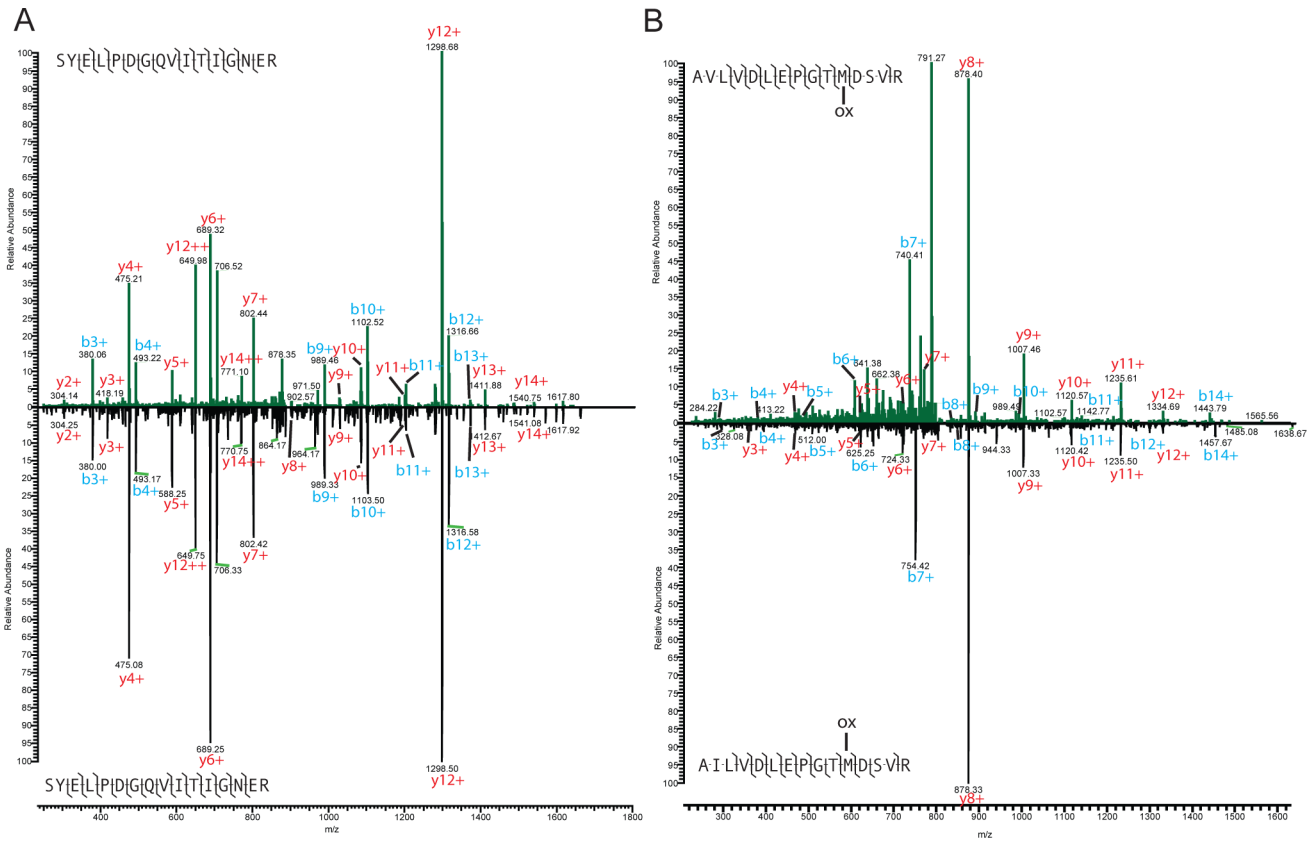

Figure 2. (A) Actin peptide detected for *B. canadensis* (top) and ostrich (bottom) showing the same fragmentation pattern. (B) Beta tubulin peptides from *B. canadensis* (AVLVDLEPGTMDSVR; top) and ostrich (AILVDLEPGTMDSVR; bottom). The second position (V vs I) is different between the peptides, and the fragmentation difference is observable as a ~14 Da mass shift. Both peptides show methionine oxidation (ox). The *B. canadensis* peptide was detected in the 12T Velos FT-ICR after fragmentation using CID, and the ostrich peptide was detected in the LTQ Orbitrap XL after fragmentation using CID.

```
---------- ---------- ---------- ---------M LMSILPQPAM
DEEIAALVVD NGSGXCKAGF AGDDAPRAVF PS-------- -----VGMGQ
KDSYVGDEAQ SK-------- ---------- ---------- ------VAPE
EHPILL---- ---------M TQIMFETFNT PAMYVAIQAV LSLYASGR--
---------- ---------- ---------- ----D----L TDYLMK----
-GYSFTTTAE E----DIKEK LC---YVALD FEQEMATAAS SSSLESSYEL
PDGQVITIGN ---------- ERFRCPEALF QPS------- ----------
---------D LYANTVLSGG TTMYPGIADR MQEEITALAP STMK--IIAP
PERKYSVWIG GSILASLSTF QQMWISKQEY DESGPSIVHR K--
```

Figure 3. Partial *B. canadensis* actin sequence derived from alignment of the detected peptides against archosaurian and testudine actin sequences.

set to 2.17, and gamma was set to 0.29, allowing for direct, quantifiable comparison with ostrich tissues.

Cotton Blue Staining

B. canadensis sections (200 nm) were taken on an ultramicrotome as described above and were stained on microscope slides using the lactophenol cotton blue solution protocol from the manufacturer (Fluka Analytical). Control unembedded samples of modern fungus were used as a positive control for this assay.

Paleohistological Preparation

To demonstrate minimum alteration of bone microstructure, which may favor preservation of endogenous organic content, cortical bone fragments were embedded in Silmar resin, cut, and ground following previous protocols[42] for histological analyses. Light images were taken on a Zeiss Axioskop 2, and cross-polarized images were taken on a Zeiss Axioskop 40.

RESULTS

Protein Extraction

For the *B. canadensis* guanidine HCl extraction, protein pellets ranging in size from 0.4 to 1.2 mg were obtained, depending on the method of extraction.[43] The sediment and buffer controls produced significantly smaller pellets, ranging between <0.1 and 0.5 mg. For extant controls, pellets ranged in size from <0.1 to 0.2 mg. Although the measured mass from the *B. canadensis* was greater than the extant pellets, the majority of material precipitating after extraction is likely to be nonproteinaceous.

DOI: 10.1021/acs.jproteome.5b00675
J. Proteome Res. 2015, 14, 5252−5262

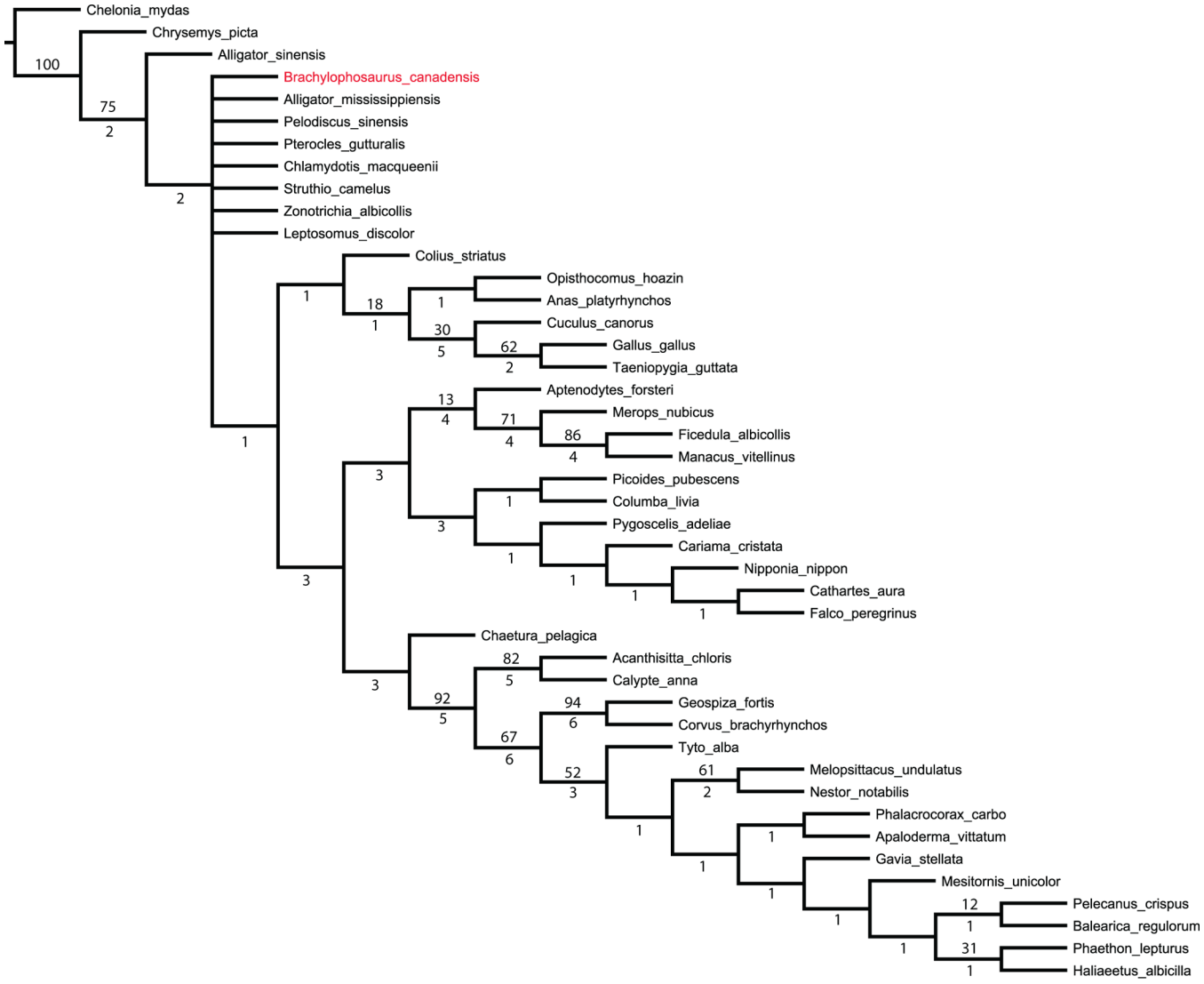

Figure 4. Maximum parsimony phylogeny derived from myosin sequences. Jackknife values are given above branches, and Bremer support, below branches.

Mass Spectrometry

Sequences of peptides from various vessel proteins were detected only in the guanidine HCl fraction of extracted *B. canadensis* blood vessels using high-resolution mass spectrometry (Tables S4 and S5) and represent some of the most abundant proteins in blood vessels.[30] These include peptides from actin (Tables S4 and S5 and Figures 2A and S1–S7); alpha and beta tubulin (Tables S4 and S5 and Figures S8–S10); histones H2A, H2B, and H4 (Tables S4 and S5 and Figure S11); myosin (Tables S4 and S5 and Figure S12–S28); and tropomyosin (Tables S4 and S5 and Figures S29–S32). Unlike the *B. canadensis* extractions, we detected vessel peptides in all three of the extraction steps from the ostrich and chicken vessels (Tables S6–S13).

All of the *B. canadensis* proteins are eukaryotic, ruling out a bacterial source for the analyzed vessel structures. Searching the aligned sequences against various NCBI databases using a basic local alignment search test (BLAST) at the aligned protein level, we found that the novel sequences for all *B. canadensis* proteins (Figures 3 and S33–S36) more closely matched sequences from Archosauria + Testudines than those from general vertebrates, fungi, or slime molds. More specifically, the actin sequence matched with the following: Archosauria + Testudines (100%), vertebrates (100%), fungi (92%), and cellular slime molds (88%); the histone H4 sequence: Archosauria + Testudines (100%), vertebrates (100%), fungi (100%), cellular slime molds (84%); tropomyosin: Archosauria + Testudines (39%), vertebrates (24%), fungi (0%), cellular slime molds (0%); the tubulin beta sequence: Archosauria + Testudines (100%); vertebrates (75%), fungi (75%), cellular slime molds (63.8%); and the myosin sequence: Archosauria + Testudines (32%), vertebrates (21%), fungi (17%), cellular slime molds (12%). The *B. canadensis* myosin sequence places it in the basal part of the archosaurian tree between *Alligator sinensis* and birds (Figure 4); however, the addition of less conserved sequences may provide more resolution of its exact molecular phylogenetic placement.

Many peptides from collagen I were detected from the ostrich and chicken extractions even though these bones had been previously digested with collagenase.[21] We do not observe collagen I peptides in the *B. canadensis* because we separated the vessels from the residual collagenous matrix before extraction. Most of the *B. canadensis* proteins were also

DOI: 10.1021/acs.jproteome.5b00675
J. Proteome Res. 2015, 14, 5252–5262

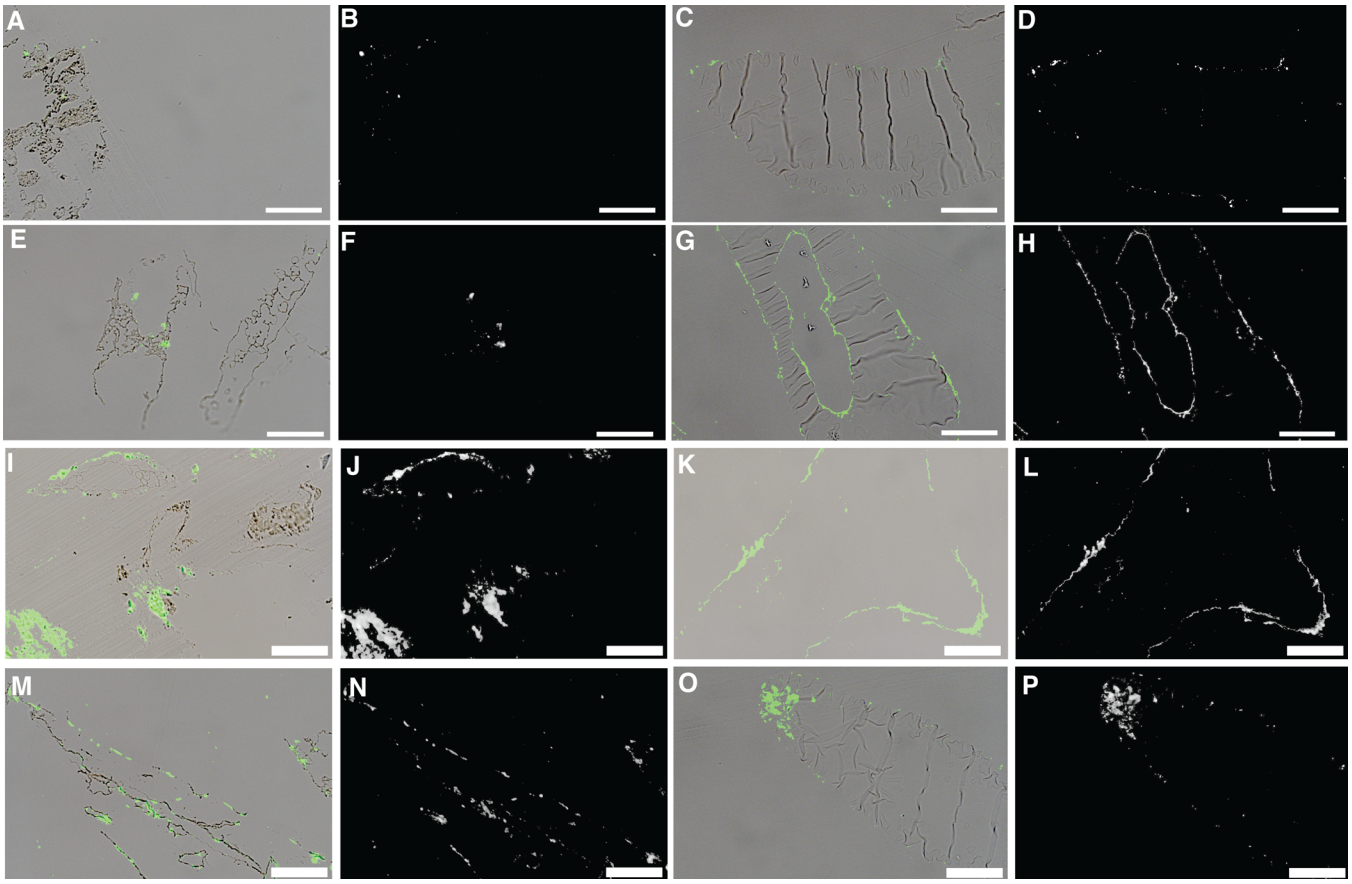

Figure 5. Immunological staining of *B. canadensis* (A, B, E, F, I, J, M, N) and ostrich (C, D, G, H, K, L, O, P) vessels, using antibodies raised against chicken tubulin (A–D), chicken actin (E–H), bovine myosin (I–L), and chicken tropomyosin (M–P). Scale bars are 20 μm. See Table S2 for detailed description of antibodies and dilutions used in this study.

detected in the extant comparative analogs (Table S20). Sequence differences were observed between *B. canadensis* and ostrich peptides, supporting the endogeneity of these sequences and rejecting potential cross-contamination (Figure 2B).

Buffer controls show only normal laboratory contamination, (e.g., keratin, trypsin), accounted for in database search algorithms (Tables S14–S18). Sedimentary controls have bacterial peptides (e.g., from elongation factor tu) and other normal contamination (Tables S14–S18), but peptides recovered from analyzed *B. canadensis* vessels were *not* identified in coextracted sediments. Laboratory contaminants (e.g., keratin, trypsin) from the sediment and buffer controls were also observed for the *B. canadensis* extracts. Additionally, environmental signals (e.g., elongation factor tu) consistent with burial environments were observed in *B. canadensis* extractions.

Comparison of PEAKS7 and Byonic results shows overlap between the two methods (Figure S37), with most of the discrepancies being the result of variable post-translational modification placements (all PEAKS7 FDR values are included in Table S18). We detected the following PSMs vs MS/MS spectra: *B. canadensis*, 380/7598; buffer control, 369/6334; sediment control, 90/5890; ostrich, 2264/9686; and chicken, 5638/37527.

Deamidation values (Table S19) ranged from 20.13 to 85.85%QN (average: 43.88 ± 17.27%). For actin, the average deamidation was 47.19 ± 18.14%; for histone H2A, the average deamidation was 43.68 ± 32.72%; and for myosin, the average deamidation was 39.52 ± 14.01%.

Immunofluorescence

All primary antibodies (Table S2) tested on *B. canadensis* tissues showed positive reactivity comparable in pattern to that seen in extant controls but with reduced signal (Figure 5). Anti-human testosterone (Figure S38I–L) was negative for both *B. canadensis* and extant controls, as expected. Secondary antibodies (Figure S38E–H) were also negative; no nonspecific binding was seen in either *B. canadensis* or extant controls. Significantly, each primary antibody applied to ancient tissues showed binding patterns distinct from one another, but the patterns seen in ancient samples were similar to the patterns seen in the corresponding extant control, lending additional support to the specificity of the reaction with dinosaur vessels in situ. Within the cytoskeleton of the vessels, tubulin (Figure 5A–D), actin (Figure 5E–H), myosin (Figure 5I–L), and tropomyosin (Figure 5M–P) were detected along the vascular margins. When primary antibodies were inhibited by incubation with excess actin (Figure S38A,B) and tubulin (Figure S38C,D) and then incubated with the *B. canadensis* tissues, signal was reduced, again supporting the specificity of these primary antibodies and endogenous origin of the signal.

Cotton Blue Staining

No cotton blue staining was observed on the *B. canadensis* tissue (Figure S39, left); however, extensive staining was observed for the fungal control (Figure S39, right).

DOI: 10.1021/acs.jproteome.5b00675
J. Proteome Res. 2015, 14, 5252–5262

Paleohistology

Ground sections of *B. canadensis* bone showed retention of the fibrolamellar bone structure expected for this dinosaur, including osteons, osteocyte lacunae, vascular canals, and interstitial woven bone (Figure S40). Additionally, we observed no evidence of bacterial or fungal invasion and no evidence of recrystallization based on cross-polarized birefringence of the structures.[44]

DISCUSSION

Previous analyses of dinosaur peptides and soft tissues have been criticized as potentially arising from unknown contamination,[2] from biofilm,[26] or being statistically insignificant,[3] leading to questions of their endogeneity. We employed a highly refined methodology to minimize sources of contamination (e.g., using separate laboratories for preparation of extant and *B. canadensis* protein extracts and vessels; analyzing dinosaur peptides on instruments that had never been exposed to any avian proteins; employing extensive personal protective equipment to reduce human contamination that included nitrile gloves, lab coats, hair coverings, laminar flow hoods, and a dedicated "ancient" processing room) and to increase statistical significance (i.e., using multiple algorithms for searching with 1% FDR). This methodology was also used to exclude the presence of bacterial or fungal molecules or their microscopic traces in the *B. canadensis* blood vessels or bone (e.g., paleohistological analysis examining for microbial invasion, comprehensive database searching, BLAST searching, *B. canadensis* protein sequence alignments, cotton blue staining) to support the endogeneity of the identified peptides. We identified cytoskeletal and nuclear peptide sequences (190 PSMs) from 10 different proteins (Tables S4 and S5). These proteins/peptides were not found in mass spectrometry analyses of the sediments extracted in tandem with the bone or in buffer controls, supporting their endogeneity to *B. canadensis* blood vessels. Furthermore, the proteins identified by mass spectrometry were validated by localized binding of antibodies raised against the same proteins to dinosaur vessels (Figure 5). Although the specificity of antibodies has been questioned when they are applied to fossils,[21] appropriate negative controls and differential binding patterns testify to their specificity. We evaluated our in situ immunofluorescence results using multiple negative controls consisting of (1) no primary antibody, but all other steps identical to the test conditions (to control for nonspecific binding of secondary antibody to tissue); (2) inhibition of primary antibodies to reduce binding (to show specificity for target protein); and (3) primary antibodies raised against proteins not predicted to be present in archosaurs bone (to show primary antibodies are specific to epitopes preserved in the tissues, not random). All of these controls were negative for binding and consistent with the same controls on extant tissues. We also show that not all antibodies bind with the same pattern on *B. canadensis*; rather, they exhibit binding patterns unique to each antibody yet consistent with patterns observed in extant controls. Furthermore, the complementary and consistent nature of the mass spectrometry peptide sequence data and in situ immunofluorescence data presented here support the hypothesis that these molecules derive directly from the *B. canadensis* blood vessels and are not from environmental or laboratory contamination.

In addition, to test the hypothesis that these blood vessels are derived from a bacterial or fungal origin, we first examined the histological integrity of the *B. canadensis* bone. We found no classical evidence of microbial invasion in the bone (e.g., Wedl tunnels, focal destruction;[44] Figure S40), indicating that this specimen was minimally affected by microbial invasion. Additionally, cotton blue staining (i.e., a specific histological stain for fungi) did not stain the *B. canadensis* blood vessels, but it caused extensive staining on a fungal control (Figure S39). Fungal hyphae are also an order of magnitude smaller than the vessels, do not taper after branching, and are often septate.[45,46] None of these features are observed in dinosaur material. Furthermore, the vessels we recovered are morphologically inconsistent with biofilm produced by bacteria or fungi. Microbial biofilm is patchy in distribution and contains microbial bodies within an amorphous matrix,[47] in contrast to the continuous vessel walls with uniform thickness that we observe.

Slime molds (e.g., *Dictyostelium* spp.) are eukaryotic; thus, they could share some of the molecular features observed in the vessels. However, slime molds are superficial detritus feeders[48] and thus would not have access to bone buried for millions of years in undisturbed sediments. Furthermore, to our knowledge, slime molds have not been observed to invade buried bone. Ongoing studies show that antibodies against vessel-associated proteins do not bind to biofilm, nor do antibodies raised against peptidoglycans (a component of biofilm) bind to these vessel structures (Schweitzer et al., in review). Therefore, our antibody binding patterns are consistent with an endogenous origin, but they are not consistent with spurious binding to microbial proteins.

In addition to histological, immunological, and morphological inferences, we evaluated cytoskeletal and nuclear protein sequences recovered from *B. canadensis* vessel extracts for the presence/absence in bacteria or fungi, as similar proteins to those found in vertebrates exist in some of these organisms. A bacterial origin is immediately excluded because the proteins we detected from the *B. canadensis* blood vessels (e.g., actin, tubulin, histones) are exclusive to eukaryotes.[27,49] Although many of the peptides we report are highly conserved across all eukaryotes, sequence comparisons between aligned *B. canadensis* sequences and those of fungi or cellular slime molds show limited or no overlap. The exception is histone H4, which has very limited sequence variation in all eukaryotes. In contrast, high levels of sequence homology with Archosauria + Testudines are shown for actin, histone H4, tropomyosin, tubulin beta, and myosin (i.e., as much as 100% sequence overlap). Additionally, all of the sequences derived from dinosaur vessels show the greatest homology with archosaurs and testudines and the lowest with fungi or cellular slime molds. We utilized aligned, protein level basic local alignment searches instead of the peptide level to accommodate for the sequence homology of our proteins.

The use of two independent search algorithms (i.e., PEAKS7[31,32] and Byonic[50]) results in the same identifications (Figure S37), lending robust support to their assignments, and, together with a restrictive FDR cutoff, provides strong statistical support for our identifications. Through this multialgorithm approach, we detected PTMs in the *B. canadensis*, both those derived from diagenesis and biological ones. Diagenetic PTMs provide evidence that the peptides are ancient and do not arise from modern contamination. We detected extensive diagenetic deamidation (Table S19 and Figure S20) including variable

DOI: 10.1021/acs.jproteome.5b00675
J. Proteome Res. 2015, 14, 5252−5262

deamidation across the same peptide (e.g., IIAPPERKYSV-WIGGSILASSTQ(±)Q(±)MWISKQ(±)EYDESGPSHIVHR, where ± indicates presence/absence of deamidation). The deamidation varied from ~20 to 85%QN; however, deamidation may not represent an age signal but instead may correspond to environmental conditions of preservation.[51,52] We urge caution when interpreting deamidation values as a marker of antiquity. In contrast to Hill et al.,[53] we did not find complete or near complete deamidation for our peptides, and this may be related to differences in preservational mode between wet bone matrix and iron-mediated preservation[41] of the blood vessel proteins. Additional diagenetic protein modifications include many occurrences of backbone cleavage, a recently described diagenetic change,[54] based on the presence of nontryptic peptides (<15% of all peptides nontryptic; e.g., K.AGFAGDDAPRAVP**S**.I, K.SYELPDGQVITI**G**.N, Q.**E**YDESGPSIVHR, Y.**S**VWIGGSILASLSTFQQMWISK, where nontryptic backbone cleavage is bold and the amino acid that precedes/follows the peptide is before or after a period). Two of the backbone cleavages are directly adjacent to positions that may be deamidated, leading us to propose deamidation as an additional mechanism for diagenetic backbone cleavage beyond the previously hypothesized proline oxidation reactions.[54] The presence of these diagenetically cleaved peptides, together with noncleaved versions of *B. canadensis* peptides, provides further support for this process. We were also able to detect several biologically derived PTMs (e.g., acetylation, methylation) that, through future research, may result in a better understanding of how these proteins evolve. Both acetylation and methylation have been shown to persist in early diagenesis,[54] a critical time for preserving proteins and their modifications into deep time.

We have shown that the key to identification of less abundant proteins lies in isolating blood vessels from bone prior to extraction. Furthermore, using multiple search engines with robust cut-offs adds strength to data generated in this manner when the same peptides are identified by each search engine. Application of these approaches to other fossil specimens, derived from both Mesozoic and Cenozoic deposits, will further identify the types of proteins likely to persist into deep time or, more specifically, will identify particular functional groups or molecular characteristics that increase preservation potential. In turn, this will add to understanding of molecular diagenetic change and differentiation of in vivo and ex vivo PTMs. These data will allow predictions of protein breakdown pathways in natural environments to be made.

■ CONCLUSIONS

Our results add further, robust support to the identification of these still soft, hollow structures as remnant blood vessels produced by the once living dinosaur (e.g., Haversian and/or Volkmann's osseous vessels). High-resolution mass spectrometry applied to paleoproteomics and soft tissue analyses allow confident identification of evolutionarily significant protein and peptide sequences from extinct taxa and provide valuable molecular support for endogeneity of soft tissue structures and biomolecules, especially when coupled to in situ localization of epitopes corresponding to MS-characterized peptides using immunofluorescence. This method also identifies both diagenetic and biological PTMs, the former supporting peptide antiquity and endogeneity to the *B. canadensis* blood vessels, and the latter providing a possible means to determine pace and/or direction of evolutionary change at the molecular level as well as suggesting possible pathways for preservation. Confirming the presence of these proteins on the dinosaur vessels by employing in situ immunolocalization and a high level of histological integrity further supports that the peptides detected from *B. canadensis* blood vessels are endogeneous and not a product of bacterial or fungal contamination. When all data are taken into consideration, the most parsimonious explanation is that these vessels, derived from demineralized dinosaur bone, are endogenous. These data open the door for molecular characterization of biological components of other long-extinct organisms.

■ ASSOCIATED CONTENT

Supporting Information

The Supporting Information is available free of charge on the ACS Publications website at DOI: 10.1021/acs.jproteome.5b00675.

Annotated spectra for most of the *B. canadensis* peptides; figures of the protein alignments, Venn diagram of overlapping Byonic and PEAKS7 results, negative control immunofluorescence, cotton blue staining, and paleohistology images; tables of antibodies, proteins used for antibody inhibition, and overlap in extant control protein with the *B. canadensis* proteins; nexus file used for TNT analysis (Figures S1−S40 and Tables S2, S3, and S20, PDF)

NCBI accession numbers of proteins used for alignments (Table S1, XLS)

B. canadensis peptides, expect scores from PEAKS7 and Byonic, and detected post-translational modifications detected on the 12T Velos FT-ICR and Orbitrap Elite (Table S4, XLSX; Table S5, XLSX)

Struthio camelus peptides detected on the LTQ-Orbitrap XL (Table S6, XLSX; Table S7, XLSX; Table S8, XLSX; Table S9, XLSX)

Gallus gallus peptides detected on the LTQ-Orbitrap XL (Table S10, XLSX; Table S11, XLSX; Table S12, XLSX; Table S13, XLSX)

Sediment and buffer control peptides, expect scores from PEAKS7, and detected post-translational modifications detected on the 12T Velos FT-ICR and Orbitrap Elite (Table S14, XLSX; Table S15, XLSX; Table S16, XLSX; Table S17, XLSX)

False discovery rates for all PEAKS files and all searches (Table S18, XLSX)

Deamidation values derived from MS2 spectra using Isotopica (Table S19, XLSX)

The mass spectrometry proteomics data have been deposited to the ProteomeXchange Consortium (http://proteomecentral.proteomexchange.org) via the PRIDE partner repository[34] with the dataset identifier PXD001738. The project DOI is 10.6019/PXD001738.

■ AUTHOR INFORMATION

Corresponding Author

*E-mail: tpcleland@utexas.edu. Phone: +1-919-515-7838.

Present Address

■(T.P.C.) Department of Chemistry, University of Texas−Austin, Austin, Texas 78712, United States.

Notes

The authors declare no competing financial interest.

DOI: 10.1021/acs.jproteome.5b00675
J. Proteome Res. 2015, 14, 5252−5262

■ ACKNOWLEDGMENTS

We would like to thank J. Carlson and S. Baxter for access to the LTQ Orbitrap XL at David H. R. Murdoch Research Institute. We thank B. Harmon, J. Horner, and the Museum of the Rockies paleontology crew responsible for the recovery of and access to this specimen. We would also like to thank Scott Hartman and Lukasiniho for providing access to the *Brachylophosaurus canadensis* and *Struthio camelus* silhouettes through Creative Commons Attribution−NonCommercial ShareAlike 3.0 Unported licenses and Scott Traver for access to the *Gallus gallus* silhouette through Public Domain Dedication 1.0 license. All silhouettes were downloaded from PhyloPic.org. This research was funded by NSF EAR 0541744 to M.H.S., DGE-0750733 to T.P.C., the David and Lucile Packard Foundation to M.H.S., NSF INSPIRE to M.H.S. and E.R.S., NIH GM067193 to N.L.K.; M.B. was supported in part by NIH grant R21GM94557, M.B.D. was a 2007 UNCF/Merck Postdoctoral Fellow and supported by the Cancer Biology Training Grant (5 T32 CA081156-08) to the BIDMC. R.K. is supported by the Cancer Prevention and Research Institute of Texas and the Metastasis Research Center at MD Anderson Cancer Center, NIH grants DK55001, DK81976, CA125550, CA155370, and CA163191. The funders had no role in study design, data collection and analysis, decision to publish, or preparation of the manuscript.

■ REFERENCES

(1) Asara, J. M.; Schweitzer, M. H.; Freimark, L. M.; Phillips, M.; Cantley, L. C. Protein Sequences from Mastodon and Tyrannosaurus Rex Revealed by Mass Spectrometry. *Science* **2007**, *316* (5822), 280−285.

(2) Buckley, M.; Walker, A.; Ho, S. Y. W.; Yang, Y.; Smith, C.; Ashton, P.; Oates, J. T.; Cappellini, E.; Koon, H.; Penkman, K.; Elsworth, B.; Ashford, D.; Solazzo, C.; Andrews, P.; Strahler, J.; Shapiro, B.; Ostrom, P.; Gandhi, H.; Miller, W.; Raney, B.; Zylber, M. I.; Gilbert, M. T. P.; Prigodich, R. V.; Ryan, M.; Rijsdijk, K. F.; Janoo, A.; Collins, M. J. Comment on "Protein Sequences from Mastodon and Tyrannosaurus rex Revealed by Mass Spectrometry". *Science* **2008**, *319* (5859), 33−33.

(3) Pevzner, P. A.; Kim, S.; Ng, J. Comment on "Protein Sequences from Mastodon and Tyrannosaurus rex Revealed by Mass Spectrometry". *Science* **2008**, *321* (5892), 1040−1040.

(4) Schweitzer, M. H.; Zheng, W.; Organ, C. L.; Avci, R.; Suo, Z.; Freimark, L. M.; Lebleu, V. S.; Duncan, M. B.; Vander Heiden, M. G.; Neveu, J. M.; Lane, W. S.; Cottrell, J. S.; Horner, J. R.; Cantley, L. C.; Kalluri, R.; Asara, J. M. Biomolecular Characterization and Protein Sequences of the Campanian Hadrosaur *B. canadensis*. *Science* **2009**, *324* (5927), 626−631.

(5) Ostrom, P. H.; Gandhi, H.; Strahler, J. R.; Walker, A. K.; Andrews, P. C.; Leykam, J.; Stafford, T. W.; Kelly, R. L.; Walker, D. N.; Buckley, M.; Humpula, J. Unraveling the sequence and structure of the protein osteocalcin from a 42 ka fossil horse. *Geochim. Cosmochim. Acta* **2006**, *70* (8), 2034−2044.

(6) Buckley, M.; Anderung, C.; Penkman, K.; Raney, B. J.; Götherström, A.; Thomas-Oates, J.; Collins, M. J. Comparing the survival of osteocalcin and mtDNA in archaeological bone from four European sites. *Journal of Archaeological Science* **2008**, *35* (6), 1756−1764.

(7) Buckley, M.; Collins, M.; Thomas-Oates, J.; Wilson, J. C. Species identification by analysis of bone collagen using matrix-assisted laser desorption/ionisation time-of-flight mass spectrometry. *Rapid Commun. Mass Spectrom.* **2009**, *23* (23), 3843−3854.

(8) Buckley, M.; Whitcher Kansa, S.; Howard, S.; Campbell, S.; Thomas-Oates, J.; Collins, M. Distinguishing between archaeological sheep and goat bones using a single collagen peptide. *Journal of Archaeological Science* **2010**, *37* (1), 13−20.

(9) Buckley, M.; Kansa, S. Collagen fingerprinting of archaeological bone and teeth remains from Domuztepe, South Eastern Turkey. *Archaeological and Anthropological Sciences* **2011**, *3* (3), 271−280.

(10) Buckley, M.; Larkin, N.; Collins, M. Mammoth and Mastodon collagen sequences; survival and utility. *Geochim. Cosmochim. Acta* **2011**, *75* (7), 2007−2016.

(11) Richter, K. K.; Wilson, J.; Jones, A. K. G.; Buckley, M.; van Doorn, N.; Collins, M. J. Fish 'n chips: ZooMS peptide mass fingerprinting in a 96 well plate format to identify fish bone fragments. *Journal of Archaeological Science* **2011**, *38* (7), 1502−1510.

(12) Waters, M. R.; Stafford, T. W.; McDonald, H. G.; Gustafson, C.; Rasmussen, M.; Cappellini, E.; Olsen, J. V.; Szklarczyk, D.; Jensen, L. J.; Gilbert, M. T. P.; Willerslev, E. Pre-Clovis Mastodon Hunting 13,800 Years Ago at the Manis Site, Washington. *Science* **2011**, *334* (6054), 351−353.

(13) Cappellini, E.; Jensen, L. J.; Szklarczyk, D.; Ginolhac, A.; da Fonseca, R. A. R.; Stafford, T. W.; Holen, S. R.; Collins, M. J.; Orlando, L.; Willerslev, E.; Gilbert, M. T. P.; Olsen, J. V. Proteomic Analysis of a Pleistocene Mammoth Femur Reveals More than One Hundred Ancient Bone Proteins. *J. Proteome Res.* **2012**, *11* (2), 917−926.

(14) Schweitzer, M.; Hill, C. L.; Asara, J. M.; Lane, W. S.; Pincus, S. H. Identification of Immunoreactive Material in Mammoth Fossils. *J. Mol. Evol.* **2002**, *55* (6), 696−705.

(15) Schweitzer, M. H.; Suo, Z.; Avci, R.; Asara, J. M.; Allen, M. A.; Arce, F. T.; Horner, J. R. Analyses of Soft Tissue from Tyrannosaurus rex Suggest the Presence of Protein. *Science* **2007**, *316* (5822), 277−280.

(16) Nielsen-Marsh, C. M.; Ostrom, P. H.; Gandhi, H.; Shapiro, B.; Cooper, A.; Hauschka, P. V.; Collins, M. J. Sequence preservation of osteocalcin protein and mitochondrial DNA in bison bones older than 55 ka. *Geology* **2002**, *30* (12), 1099−1102.

(17) Humpula, J. F.; Ostrom, P. H.; Gandhi, H.; Strahler, J. R.; Walker, A. K.; Stafford, T. W.; Smith, J. J.; Voorhies, M. R.; Corner, R. G.; Andrews, P. C. Investigation of the protein osteocalcin of Camelops hesternus: Sequence, structure and phylogenetic implications. *Geochim. Cosmochim. Acta* **2007**, *71* (24), 5956−5967.

(18) Nielsen-Marsh, C. M.; Richards, M. P.; Hauschka, P. V.; Thomas-Oates, J. E.; Trinkaus, E.; Pettitt, P. B.; Karavanić, I.; Poinar, H.; Collins, M. J. Osteocalcin protein sequences of Neanderthals and modern primates. *Proc. Natl. Acad. Sci. U. S. A.* **2005**, *102* (12), 4409−4413.

(19) Buckley, M. A Molecular Phylogeny of *Plesiorycteropus* Reassigns the Extinct Mammalian Order 'Bibymalagasia'. *PLoS One* **2013**, *8* (3), e59614.

(20) Orlando, L.; Ginolhac, A.; Zhang, G.; Froese, D.; Albrechtsen, A.; Stiller, M.; Schubert, M.; Cappellini, E.; Petersen, B.; Moltke, I.; Johnson, P. L. F.; Fumagalli, M.; Vilstrup, J. T.; Raghavan, M.; Korneliussen, T.; Malaspinas, A.-S.; Vogt, J.; Szklarczyk, D.; Kelstrup, C. D.; Vinther, J.; Dolocan, A.; Stenderup, J.; Velazquez, A. M. V.; Cahill, J.; Rasmussen, M.; Wang, X.; Min, J.; Zazula, G. D.; Seguin-Orlando, A.; Mortensen, C.; Magnussen, K.; Thompson, J. F.; Weinstock, J.; Gregersen, K.; Roed, K. H.; Eisenmann, V.; Rubin, C. J.; Miller, D. C.; Antczak, D. F.; Bertelsen, M. F.; Brunak, S.; Al-Rasheid, K. A. S.; Ryder, O.; Andersson, L.; Mundy, J.; Krogh, A.; Gilbert, M. T. P.; Kjaer, K.; Sicheritz-Ponten, T.; Jensen, L. J.; Olsen, J. V.; Hofreiter, M.; Nielsen, R.; Shapiro, B.; Wang, J.; Willerslev, E. Recalibrating *Equus* evolution using the genome sequence of an early Middle Pleistocene horse. *Nature* **2013**, *499* (7456), 74−78.

(21) Wadsworth, C.; Buckley, M. Proteome degradation in fossils: investigating the longevity of protein survival in ancient bone. *Rapid Commun. Mass Spectrom.* **2014**, *28* (6), 605−615.

(22) Schweitzer, M. H.; Wittmeyer, J. L.; Horner, J. R. Soft tissue and cellular preservation in vertebrate skeletal elements from the Cretaceous to the present. *Proc. R. Soc. London, Ser. B* **2007**, *274* (1607), 183−197.

(23) Cadena, E. A.; Schweitzer, M. H. Variation in osteocytes morphology vs bone type in turtle shell and their exceptional

DOI: 10.1021/acs.jproteome.5b00675
J. Proteome Res. 2015, 14, 5252−5262

preservation from the Jurassic to the present. *Bone* **2012**, *51* (3), 614–20.
(24) Cadena, E. A.; Schweitzer, M. H. A Pelomedusoid Turtle from the Paleocene–Eocene of Colombia Exhibiting Preservation of Blood Vessels and Osteocytes. *J. Herpetol.* **2014**, *48* (4), 461–465.
(25) Bertazzo, S.; Maidment, S. C. R.; Kallepitis, C.; Fearn, S.; Stevens, M. M.; Xie, H.-n. Fibres and cellular structures preserved in 75-million-year-old dinosaur specimens. *Nat. Commun.* **2015**, *6*, 7352.
(26) Kaye, T. G.; Gaugler, G.; Sawlowicz, Z. Dinosaurian Soft Tissues Interpreted as Bacterial Biofilms. *PLoS One* **2008**, *3* (7), e2808.
(27) Wickstead, B.; Gull, K. The evolution of the cytoskeleton. *J. Cell Biol.* **2011**, *194* (4), 513–525.
(28) Bada, J. L.; Wang, X. S.; Hamilton, H. Preservation of key biomolecules in the fossil record: current knowledge and future challenges. *Philos. Trans. R. Soc., B* **1999**, *354* (1379), 77–87.
(29) Schweitzer, M. H.; Avci, R.; Collier, T.; Goodwin, M. B. Microscopic, chemical and molecular methods for examining fossil preservation. *Comptes Rendus Palevol* **2008**, *7* (2–3), 159–184.
(30) Didangelos, A.; Yin, X.; Mandal, K.; Baumert, M.; Jahangiri, M.; Mayr, M. Proteomics Characterization of Extracellular Space Components in the Human Aorta. *Mol. Cell. Proteomics* **2010**, *9* (9), 2048–2062.
(31) Ma, B.; Zhang, K.; Hendrie, C.; Liang, C.; Li, M.; Doherty-Kirby, A.; Lajoie, G. PEAKS: powerful software for peptide *de novo* sequencing by tandem mass spectrometry. *Rapid Commun. Mass Spectrom.* **2003**, *17* (20), 2337–2342.
(32) Han, X.; He, L.; Xin, L.; Shan, B.; Ma, B. PeaksPTM: Mass Spectrometry-Based Identification of Peptides with Unspecified Modifications. *J. Proteome Res.* **2011**, *10* (7), 2930–2936.
(33) Fernandez-de-Cossio, J.; Gonzalez, L. J.; Satomi, Y.; Betancourt, L.; Ramos, Y.; Huerta, V.; Amaro, A.; Besada, V.; Padron, G.; Minamino, N.; Takao, T. Isotopica: a tool for the calculation and viewing of complex isotopic envelopes. *Nucleic Acids Res.* **2004**, *32*, W674–8.
(34) Vizcaino, J. A.; Cote, R. G.; Csordas, A.; Dianes, J. A.; Fabregat, A.; Foster, J. M.; Griss, J.; Alpi, E.; Birim, M.; Contell, J.; O'Kelly, G.; Schoenegger, A.; Ovelleiro, D.; Perez-Riverol, Y.; Reisinger, F.; Rios, D.; Wang, R.; Hermjakob, H. The PRoteomics IDEntifications (PRIDE) database and associated tools: status in 2013. *Nucleic Acids Res.* **2013**, *41*, D1063–9.
(35) Gouy, M.; Guindon, S.; Gascuel, O. SeaView version 4: A multiplatform graphical user interface for sequence alignment and phylogenetic tree building. *Mol. Biol. Evol.* **2010**, *27* (2), 221–4.
(36) Larkin, M. A.; Blackshields, G.; Brown, N. P.; Chenna, R.; McGettigan, P. A.; McWilliam, H.; Valentin, F.; Wallace, I. M.; Wilm, A.; Lopez, R.; Thompson, J. D.; Gibson, T. J.; Higgins, D. G. Clustal W and Clustal X version 2.0. *Bioinformatics* **2007**, *23* (21), 2947–2948.
(37) Goloboff, P. A.; Farris, J. S.; Nixon, K. C. TNT, a free program for phylogenetic analysis. *Cladistics* **2008**, *24*, 774–786.
(38) Maddison, W. P.; Maddison, D. R. *Mesquite: a modular system for evolutionary analysis*, version 2.75. http://mesquiteproject.org.
(39) Schweitzer, M. H.; Marshall, M.; Carron, K.; Bohle, D. S.; Busse, S. C.; Arnold, E. V.; Barnard, D.; Horner, J. R.; Starkey, J. R. Heme compounds in dinosaur trabecular bone. *Proc. Natl. Acad. Sci. U. S. A.* **1997**, *94* (12), 6291–6296.
(40) Huang, A. R.; Ponka, P. A study of the mechanism of action of pyridoxal isonicotinoyl hydrazone at the cellular level using reticulocytes loaded with non-heme 59Fe. *Biochim. Biophys. Acta, Gen. Subj.* **1983**, *757* (3), 306–315.
(41) Schweitzer, M. H.; Zheng, W.; Cleland, T. P.; Goodwin, M. B.; Boatman, E.; Theil, E.; Marcus, M. A.; Fakra, S. C. A role for iron and oxygen chemistry in preserving soft tissues, cells and molecules from deep time. *Proc. R. Soc. London, Ser. B* **2014**, *281* (1775), 1–10.
(42) Boyd, C.; Cleland, T.; Novas, F. Osteogenesis, homology, and function of the intercostal plates in ornithischian dinosaurs (Tetrapoda, Sauropsida). *Zoomorphology* **2011**, *130* (4), 305–313.
(43) Cleland, T. P.; Voegele, K.; Schweitzer, M. H. Empirical Evaluation of Bone Extraction Protocols. *PLoS One* **2012**, *7* (2), e31443.
(44) Jans, M. M. E.; Nielsen-Marsh, C. M.; Smith, C. I.; Collins, M. J.; Kars, H. Characterisation of microbial attack on archaeological bone. *Journal of Archaeological Science* **2004**, *31* (1), 87–95.
(45) Harris, S. D. Branching of fungal hyphae: regulation, mechanisms and comparison with other branching systems. *Mycologia* **2008**, *100* (6), 823–832.
(46) Bartnicki-Garcia, S.; Bracker, C. E.; Gierz, G.; López-Franco, R.; Lu, H. Mapping the Growth of Fungal Hyphae: Orthogonal Cell Wall Expansion during Tip Growth and the Role of Turgor. *Biophys. J.* **2000**, *79* (5), 2382–2390.
(47) Stoodley, P.; Boyle, J. D.; Dodds, I.; Lappin-Scott, H. M. Consensus model of biofilm structure. In *Biofilms: Community Interactions and Control*; Wimpenny, J. W. T., Handley, P. S., Gilbert, P., Lappin-Scott, H. M., Jones, M., Eds.; Bioline: Cardiff, UK, 1997; pp 1–9.
(48) Bonner, J. T.; Lamont, D. S. Behavior of cellular slime molds in the soil. *Mycologia* **2005**, *97* (1), 178–184.
(49) Nogales, E.; Downing, K. H.; Amos, L. A.; Löwe, J. Tubulin and FtsZ form a distinct family of GTPases. *Nat. Struct. Biol.* **1998**, *5* (6), 451–458.
(50) Bern, M.; Cai, Y.; Goldberg, D. Lookup Peaks: A Hybrid of de Novo Sequencing and Database Search for Protein Identification by Tandem Mass Spectrometry. *Anal. Chem.* **2007**, *79* (4), 1393–1400.
(51) Schroeter, E. R.; Cleland, T. P., Glutamine deamidation: an indicator of antiquity, or preservational quality? *Rapid Commun. Mass Spectrom.* In press.
(52) Kirby, D. P.; Buckley, M.; Promise, E.; Trauger, S. A.; Holdcraft, T. R. Identification of collagen-based materials in cultural heritage. *Analyst* **2013**, *138* (17), 4849–58.
(53) Hill, R. C.; Wither, M. J.; Nemkov, T.; Barrett, A.; D'Alessandro, A.; Dzieciatkowska, M.; Hansen, K. C. Preserved Proteins from Extinct Bison latifrons Identified by Tandem Mass Spectrometry; Hydroxylysine Glycosides are a Common Feature of Ancient Collagen. *Mol. Cell. Proteomics* **2015**, *14* (7), 1946–58.
(54) Cleland, T. P.; Schroeter, E. R.; Schweitzer, M. H. Biologically and diagenetically derived peptide modifications in moa collagens. *Proc. R. Soc. London, Ser. B* **2015**, *282*, 20150015 DOI: 10.1098/rspb.2015.0015.

DOI: 10.1021/acs.jproteome.5b00675
J. Proteome Res. 2015, 14, 5252–5262